

Helical modulation of the electrostatic plasma potential due to edge magnetic islands induced by resonant magnetic perturbation fields at TEXTOR

G. Ciaccio,^{1,*} O. Schmitz,^{2,†} G. Spizzo,¹ S. S. Abdullaev,³ T. E. Evans,⁴ H. Frerichs,² and R. B. White⁵

¹*Consorzio RFX (CNR, ENEA, INFN, Università di Padova, Acciaierie Venete SpA),
Corso Stati Uniti 4 - 35127 Padova (Italy)*

²*Department of Engineering Physics,
University of Wisconsin - Madison,
1500 Engineering Drive, Madison, WI 53706*

³*Institut für Energieforschung-Plasmaphysik,
Association EURATOM-FZJ, Jülich, Germany*

⁴*General Atomics, San Diego, California, USA*

⁵*Plasma Physics Laboratory, Princeton University,
P.O.Box 451, Princeton, New Jersey 08543*

(Dated: September 25, 2015)

Abstract

The electrostatic response of the edge plasma to a magnetic island induced by resonant magnetic perturbations to the plasma edge of the circular limiter tokamak TEXTOR is analyzed. Measurements of plasma potential are interpreted with simulations with the Hamiltonian guiding center code ORBIT. We find a strong correlation between the magnetic field topology and the poloidal modulation of the measured plasma potential. The ion and electron drifts yield a predominantly electron driven radial diffusion when approaching the island X-point while ion diffusivities are generally an order of magnitude smaller. This causes a strong radial electric field structure pointing outward from the island O-point. The good agreement found between measured and modeled plasma potential connected to the enhanced radial particle diffusivities supports that a magnetic island in the edge of a tokamak plasma can act as convective cell. We show in detail that the particular, non-ambipolar drifts of electrons and ions in a 3D magnetic topology account for these effects. An analytical model for the plasma potential is implemented in the code ORBIT, and analyses of ion and electron radial diffusion show that both ion- and electron-dominated transport regimes can exist, which are known as ion and electron root solutions in stellarators. This finding and comparison with reversed field pinch studies and stellarator literature suggests that the role of magnetic islands as convective cells and hence as major radial particle transport drivers could be a generic mechanism in 3D plasma boundary layers.

PACS numbers: 52.20.Dq,52.65.Cc

*Electronic address: giovanni.ciaccio@igi.cnr.it

†Electronic address: oschmitz@wisc.edu

I. INTRODUCTION

Plasma flows along magnetic field lines under conditions of spontaneous self-organization are a generic question in space and terrestrial plasma physics [1, 2]. In magnetically confined high temperature plasmas explored for future fusion energy production, such directed plasma flows are responsible for transport in the plasma edge. By this, the magnetic field topology in the plasma edge and the resulting transport characterizes the interface of the plasma to the surrounding neutral gas. One form of such self-organized 3D magnetic structures are magnetic islands. Field lines can be easily perturbed in a resonant way by magnetic field perturbations with the same mode structure as the rational surface of these field lines. In tokamaks, this form of resonant magnetic perturbation (RMP) is used to control plasma edge transport and stability to Edge Localized Modes (ELMs) in various devices, such as DIII-D [3], TEXTOR [4], JET [5], ASDEX Upgrade [6], NSTX [7], MAST [8] and KSTAR [9]. In EAST, a chaotic edge layer is induced via lower hybrid injection [10]. A review of RMP control issues can be found in Refs. [11, 12]. Contrary to tokamaks, in stellarators and reversed-field pinches (RFPs), islands often occur naturally as the result of a self-organized, MHD process [13]. In the edge of most of these devices, it has been reported of macroscopic modulations with the symmetry of the dominant magnetic islands. These modulations are observed in the electron density and temperature [14, 15], electron pressure [16, 17, 18, 19], and connection length [20], in presence of 3D fields and magnetic chaos in the edge. Moreover, it has been shown that magnetic islands influence the sign of the plasma flow, v , and the related radial electric field, E^r [16, 17, 19, 21, 22, 23]. This is an outstanding issue for ELM control and suppression via RMPs. In fact, ELMs are sensitive to the edge pressure gradient p' [24], and to date there is no obvious (or completely understood) relationship between p' and the magnetic perturbation. The presence of strong plasma flows further complicates this relationship, adding a strong convective term to usual diffusion.

This is an issue, for example in ITER, for the envisaged ELM control via RMP [25], but also in stellarators, where low-order rational surfaces in the periphery make them prone to island formation which in some devices is used deliberately as an exhaust layer between the plasma core and the material wall elements around the plasma [26].

The key mechanism governing the electrostatic response to edge islands is that *particle drifts depend on Larmor radius*: electrons stream along the field lines, while ions have larger

mass and, hence, larger shift of the drift orbit from the flux surface. This results in an ambipolar field, with the same symmetry as the main magnetic island, to balance the drifts and ensure quasi-neutrality. This mechanism has been often neglected, on the assumption that electron drifts are small, as stated e.g. in the review by Callen [27]: therefore, it has been considered only in stellarators, where ion banana drifts are huge, and cause a large, negative E^r to appear. On the contrary, in this paper we present a direct algebraic determination of an ambipolar potential in a tokamak with resonant magnetic perturbation fields applied, using the same tools which are customary in the stellarator community to determine the sign and magnitude of the radial electric field E^r [28]. We will show that the mechanism of ambipolarity allows for two possible solutions ("roots"), which suggests a way of acting on the edge E^r through additional heating. The paper is organized as follows: Section II describes the TEXTOR device and measurements of electrostatic potential in correspondence with edge islands, while Section III sets the theoretical framework for the study. Sections IV,V are dedicated to ORBIT simulations: Section IV discusses electron/ion transport with and without a model of ambipolar potential, and discusses similarities between the measured and modeled potential maps. Section V discusses the stability of the ambipolar solution as a function of the edge radial electric field E^r . In Section VI we draw our conclusions.

II. EXPERIMENTAL SETUP

We study a circular shaped, high field side limited plasma at the TEXTOR tokamak [29], where RMPs are induced by the Dynamic Ergodic Divertor (DED) [30]. During RMP application at TEXTOR, in general two plasma boundary configurations can be differentiated. First, formation of a so-called laminar zone where interleaved short and long connection length magnetic field lines in the stochastic layer form a set of correlated magnetic flux bundles of different wall to wall connection length [31, 32, 33, 34, 35]. This configuration represents a helical scrape-off layer (SOL) and features reduced particle confinement when the dominant resonance layer is located inside of the ionization source [36] but can also yield improved particle confinement when the resonant surface is moderately perturbed [36, 37, 38]. The second configuration is that of a magnetic island being present in the plasma edge. This can be realized reproducibly at TEXTOR and we report in the following of the influence of this edge magnetic island on helium exhaust. We discuss a class of

TEXTOR discharges with the following typical plasma parameters: toroidal magnetic field $B_t = 1.9T$, plasma current $I_P = 350kA$, ohmic heating power $P_{OH} = 320kW$, neutral beam heating power $P_{NBI} = 2.2MW$, DED current $I_{DED} = 1.8kA$ with $m/n = 3/1$ base mode configuration, edge safety factor $q_a = 4.5$, central plasma density $n_{e,0} = 3.4 \times 10^{19}m^{-3}$.

The presence of the island is identified by a variety of signatures which are described in detail in [39]. For instance a direct image of the island separatrix has been obtained in the light of double ionized carbon right in front of the DED target. The location and size of the $m/n = 4/1$ contours of an island located on the $q = 4$ surface at $r/a = 0.92$ are mapped out along isothermal flux surfaces in the island boundary and a fair agreement with vacuum field modeled island size and location has been found. In addition to the spectroscopic signal we also measured for the first time at TEXTOR the plasma potential in the vicinity of the island. The experimental data is presented in Figure 1. To achieve this measurement we used the capacity of the DED to shift the current maximum from one coil quadruple to the adjacent one which was also used to map out plasma parameters in the laminar zone of TEXTOR-DED [35]. This yields a movement of the island O-point at the low field side of TEXTOR by $\Delta\theta = 15$ degrees poloidally. Accordingly, we can sample the radial profiles of the plasma potential with the reciprocating Langmuir system at the low field side of TEXTOR and obtain a poloidal map of the plasma potential from the X- to the O-point of the island. The map of the plasma potential in the laboratory frame of reference is shown in Figure 1, as a function of the radial distance from the last closed flux surface (LCFS) on the x-axis, and the poloidal "steps" of the DED on the y-axis. A clear increase of the plasma potential from $\approx 30V$ in the very edge of the plasma to $\approx 90V$ in the island O-point is measured. This transfers to a positive radial electric field $E_{isl} = 0.2 - 2$ kV/m across the island domain pointing outwards the island's O-point, with possible significant impact on particle transport due to increased radial and poloidal drifts. Qualitatively this is in agreement with the robust experimental observation that in the configuration with edge magnetic island present in the plasma ionization region, particle transport is largely enhanced and particle fueling is reduced. Also, this configuration features screening of carbon impurities released from the wall [40], which is consistent with a strong, positive radial electric field. The goal of this paper is to understand the link between the plasma potential structure bound to the magnetic island topology and particle transport during RMP application in TEXTOR.

The particle transport properties of the magnetic topology in the DED configuration $m/n = 12/4$ were already analyzed using Poincaré plots and by calculating the parallel connection length, L_{\parallel} , for ions and electrons. These simulations make use of the Hamiltonian, guiding-center code ORBIT [41]. The resulting L_{\parallel} map showed a radial and poloidal modulation, being footprints of the magnetic topology [42]. Results with ORBIT are consistent with maps of connection length made with field line tracing using the vacuum field approximation and a axisymmetric plasma equilibrium [35]. Previous results have pointed to the formation of island convective cells due to $\vec{E} \times \vec{B}$ flows around magnetic islands [43, 44, 45, 46]. Here, we show for the first time that ambipolar potentials, with the same symmetry as the magnetic island, due to differential drifts of ions and electrons in islands can account for the radial electric fields responsible for these flows. This potential is the response of the plasma to non-ambipolar fluxes, generated through the breaking of the toroidal symmetry by the 3D fields. Similar results have been obtained in the RFX-mod RFP, where a model of electrostatic potential was built up for the island resonating with poloidal/toroidal mode number $m/n = 0/1$ at the edge of RFX-mod [47]. This model reproduces the main features of E^r , such as amplitude and geometry along the toroidal angle φ . The modulation of E^r generates a convective cell pattern which is being considered as a possible contributor to the empirical density limit (Greenwald limit) [48, 49]. In Sections IV–V we will complete and generalize the model developed at RFX, in the case of RMPs in a Tokamak configuration. In particular, we will analyze electron/ion diffusivities in helical coordinates (Section IV) and we will develop an analytical model of ambipolar potential, to insert into ORBIT transport simulations. In Section V we will evaluate electron/ion fluxes in presence of this potential, and adjust the free parameters (amplitude and phase) in order to ensue ambipolarity. The amplitude scan (never done before on RFX) will reveal the presence of two possible solutions to the equation of flux balance $\Gamma_e = \Gamma_i$: these are the "roots" in stellarator jargon. Concluding remarks on how additional heating could possibly modify this picture will be presented in Section VI.

III. THEORETICAL BASIS

As anticipated in the Introduction, the studies we present in this paper show an analogy with the theory of the neoclassical response to magnetic islands in the stellarator [27],

where banana trajectories do not close onto themselves on the poloidal plane, due to the 3D distortion [50, 51]. Nevertheless, there is a single, fundamental difference: in our case, the engine of the response is the increased electron mobility at the X-points of the edge islands. This effect was neglected in the past [27] on the assumption that electron drifts are small (which is correct in the stellarator without a stochastic edge). On the contrary, in the case of a stochastic edge, such as in TEXTOR, the tiny details of stochastic layers and fixed points dominate over neoclassical effects in driving transport, and an optimal tool is a guiding-center (GC) code, such as ORBIT [41]. ORBIT has an Hamiltonian formulation of the GC equations of motion, plus the additional capability of describing collisional effects for electrons/ions, through a Monte-Carlo package based on the Boozer-Kuo operator [52]. A heuristic argument for demonstrating the need of a potential Φ to balance the asymmetry of electron/ion fluxes in presence of a 3D perturbation, can be derived directly from the GC equations. Specify the equation for electrons and ions [53], and neglect the ripple:

$$\dot{P}_\zeta^{(e)} = \rho_\parallel^e B^2 \partial_\zeta \alpha + \frac{\partial \Phi}{\partial \zeta} \quad (1)$$

$$\dot{P}_\zeta^{(i)} = \rho_\parallel^i B^2 \partial_\zeta \alpha - \frac{\partial \Phi}{\partial \zeta} , \quad (2)$$

where $\rho_\parallel = mv_\parallel/eB$ is the “parallel” gyro-radius, P_ζ is the canonical toroidal momentum, and the magnetic field perturbation is treated as $\delta \vec{B} = \nabla \times \alpha \vec{B}_0$. Flux coordinates of Boozer-type (ψ_p, θ, ζ) are used. The meaning of Eqs. (1-2) is that, in presence of a 3D field α , the toroidal momentum P_ζ is no more conserved in time. On the other hand, a larger drift (larger ρ_\parallel^i) for ions determines a different response to the symmetry breaking brought about by $\partial_\zeta \alpha$, and this different change in \dot{P}_ζ must be balanced by the ambipolar potential Φ . Subtract (1) from (2)

$$\dot{P}_\zeta^{(i)} - \dot{P}_\zeta^{(e)} = (\rho_\parallel^i - \rho_\parallel^e) B^2 \partial_\zeta \alpha - 2 \frac{\partial \Phi}{\partial \zeta} = 0 , \quad (3)$$

and solve in terms of the potential

$$\frac{\partial \Phi}{\partial \zeta} = \frac{1}{2} (\rho_\parallel^i - \rho_\parallel^e) B^2 \partial_\zeta \alpha . \quad (4)$$

If α is a single mode, $\alpha = \alpha_{m,n} \sin(m\theta - n\zeta + \phi)$, with ϕ phase of the mode, Eq. (4) can be integrated to give

$$\Phi(\psi_p, \theta, \zeta) = \Phi_0(\psi_p) + \frac{1}{2} (\rho_\parallel^i - \rho_\parallel^e) B^2 \alpha_{m,n}(\psi_p) \sin u , \quad (5)$$

where $u = m\theta - n\zeta + \phi$ is the helical angle. This heuristic argument does not catch the overall complexity of the electron and ion motion (full ORBIT simulations are needed), but it shows that, whenever you break the symmetry, this is done differently for electrons and ions, and a balancing Φ is needed, which will be modulated as $\sin u$. This is independent of the shape of the equilibrium flux surfaces ψ_p , and it is valid also for slowly rotating islands, where $u = m\theta - n\zeta + \omega t$.

IV. MAPS OF PLASMA POTENTIAL: EXPERIMENTS AND SIMULATIONS

The experiments on TEXTOR which are used in this paper have been performed in the L-mode wall limited circular plasmas, with a mode number resonant field $m/n = 3/1$ (“base” mode) produced with the DED (see Section II). As already extensively described elsewhere [35], the 3/1 MP produces a series of higher harmonics (“sidebands”), including a chain of secondary islands with periodicity 4/1 resonating well in the edge, at $r/a \sim 0.9$. The numerical interpretation was conducted using test particle transport simulations by means of ORBIT. We calculate the particle diffusion coefficients for electrons, D_e , and ions, D_i , and develop a model for the ambipolar potential to insert into transport simulations, which describes the two-fluid, plasma response to the RMP. In this Section we will show that the modeled potential reproduces quite well the measurements of Figure 1. The results demonstrate that the development of an electrostatic potential is a general feature of magnetic islands resonating at the plasma edge: moreover, two possible ambipolar solutions are present, which resemble the “ion” and “electron-roots” typical of the E^r in stellarators [28]. A consequence is that modifying the T_e/T_i ratio can let the system flip from one solution to the other.

In Fig. 2 we show the Poincaré plot of the vacuum magnetic field lines, superimposed to the helical 4/1 flux surfaces, $\psi_h^{(4,1)}$ [54], used for the computation domain and displayed as blue curves. We can recognize the characteristic magnetic topology of TEXTOR at the edge [35]: in the inner region the last main island chain composed by three conserved structures (green points), in the middle four *remnant islands* (purple points) and in the outermost region the *laminar flux tubes* embedded into the *stochastic fingers*. In Ref. [47] we presented the calculation of the particle diffusion coefficients, D , in between fixed points, O and X (OP and XP in the remainder of the paper). Here, we propose again the result

as it is instrumental to the measurements of plasma potential and the modeled ambipolar potential, that we present below. D is calculated in an helical domain centered at the $q = 4$ resonance, ($r \approx 36$ cm), and bounded by $\psi_h^{(4,1)}$, highlighted in orange and light green in Fig. 2, respectively, which can be shifted from the OP towards the XP by varying the phase, ϕ , of $\psi_h^{(4,1)}$. We considered temperature $T_e = 90$ eV and $T_i = 100$ eV and thermal collisions with a background at density $n_e = 8.7 \times 10^{12}$ cm⁻³. These values are chosen to approximate the experiment conditions and calculated through the transport code EMC3-Eirene [55] in unperturbed conditions. The area of the domain is an *Archimedes' serpentine*, namely, a cyclic helical surface generated by the helical motion of a circle, whose area is $\mathcal{A} = 4\pi^2 b \sqrt{r_s^2 + R^2 q^2}$. In the formula, b is the radius of the circle normal to the helix, r_s is the resonance radius, and R the major radius. Diffusivities are calculated in the local domain, bounded by the OP and $\psi_h^{(4,1)}$, through an analytical formula (Eq. (1) in Ref. [56]) which takes into account also a “pinch” velocity. This velocity can be large, especially in the case of fast electron transport in the stochastic domain of the XP.

D_e and D_i are shown in Fig. 3 as a function of the helical angle $u_{4,1} = 4\theta - \zeta + \phi$ [17], with θ and ζ the general poloidal and toroidal angle, respectively ($\zeta = \varphi - \nu(\psi_p, \theta)$, with ν required to fulfill the straight-field line condition in Boozer coordinates [57]). Fig. 3 is adapted from Fig. 6 in Ref. [47]. Some D_e values have been corrected (D_e curve is smoother), but the overall result does not change. D_i is rather constant along the path (≈ 0.1 m²/s), while D_e is larger, with typical values in a stochastic field [58] ($0.6 \div 40$ m²/s). More important, D_e is strongly modulated along u (larger at the XP, lower at the OP), consistently with the L_{\parallel} simulations in Ref. [42], and the well-known experimental result that the laminar flux tubes (XP of the 4/1 island) are pathways of enhanced electron diffusion [35].

To compare the measured plasma potential with ORBIT simulations, it is useful to remap the measurements of Figure 1 onto the island flux surfaces. This is shown in Fig. 4, where the measured plasma potential V_p is plotted in the (r, θ) plane, together with the helical flux surfaces $\psi_h^{(4,1)}$ and the magnetic field Poincaré map. A very clear correlation of the V_p shape with the magnetic topology is found. In particular, the correlation is very strong in the region outside the LCFS, while inside V_p does not follow exactly the flux surfaces. On the basis of the simulations of D and the measured V_p map, we find good reason to assume that the ambipolar potential Φ should possess the same geometry as the 4/1 island, similarly to the 0/1 and 1/7 island cases in RFX-mod [17, 47].

We now want to understand the link between the high electron diffusivity and the electric field structure. We will use the algebraic determination of the ambipolar electric field, which is customary in the stellarator community: some examples include FORTEC-3D [59, 60] and EUTERPE-GSRAKE [61], or the linearized drift-kinetic equation, such as in the case of DKES-PENTA [62]. In the chaotic transport calculations with ORBIT it is easier to find a proper analytic form for Φ to stick into the GC equations of motion, Eqs (1,2). To do that, we need to mix an experimental radial profile and simulation observations along θ , as previously done on RFX-mod [47]. In this way,

$$\Phi(\psi_p, \theta, \zeta) = \Phi_0 \left(f_1 + \frac{1}{2}(f_2 - f_1) \sin(-m\theta + n\zeta + \tilde{\phi}) \right), \quad (6)$$

where

$$f_i(\psi_p) = V_{p,i}^{min} + \frac{1}{2}(V_{p,i}^{max} - V_{p,i}^{min}) \times \left(1 - \tanh\left(\frac{\psi_p - \psi_{p,i}}{\Delta\psi_{p,i}}\right) \right), \quad (7)$$

with $i = (1, 2)$. f_1 and f_2 are the curves fitting the radial profile of V_p (normalized to $\langle V_p \rangle \approx 85 V$ in the OP) at the poloidal positions of the XP ($V_{p,1}^{min} = 0.35$, $V_{p,1}^{max} = 0.94$, $\psi_{p,1} = 0.0145$, $\Delta\psi_{p,1} = 0.0005$) and the OP ($V_{p,2}^{min} = 0.41$, $V_{p,2}^{max} = 1.00$, $\psi_{p,2} = 0.0148$, $\Delta\psi_{p,2} = 0.0003$), respectively. By setting $\Phi_0 = 90 V$ (the maximum amplitude in the measurements) and $\tilde{\phi} = \phi$, i.e. the same phase of $\psi_h^{(4,1)}$, we obtain a model Φ , identical to the measured plasma potential, as shown in Fig. 5. Differences between the modeled and measured potential maps are $< 10\%$ everywhere, but a small, localized spot just above the XP, at $r/a \sim 0.94$ and $\theta = 0$, where the difference is $\sim 30\%$. This happens because the modeled potential shows a steeper radial gradient above the XP, which will be matter of future investigations. This is not surprising, considering the radial modulation of Φ which coincides by construction with measurements; but the fact that the poloidal dependence follows the geometry of the island is a striking new result in the tokamak. This behavior was already found instead in the reversed-field pinch RFX-mod [17], and in gyrokinetic simulations in stellarators [61]. In Fig. 6, we map the $E^r = -\partial\Phi/\partial r$ amplitude together with the flux surfaces $\psi_h^{(4,1)}$ and magnetic field Poincaré plot, noting that E^r is modulated *both in the radial and in the poloidal directions*. In particular, a region of large positive E^r , along the LCFS, can be noticed. This is a confirmation of the well-known presence of a positive E^r in the stochastic edge of a tokamak [22, 23, 38, 63, 64, 65, 66, 67, 68]. But, if we focus on this region, we can note also a modulation in the poloidal angle, strictly linked to the magnetic topology, too: E^r has a minimum in between the XP and the OP,

and an absolute maximum in correspondence of the XP. On the contrary, right into the OP, E^r almost vanishes, which is consistent with LHD results [46, 69] and the fact that $D_e \approx D_i$ in the island OP (see Figure 3). Therefore, the potential well is located near the XP, where the electrons are preferably lost, as shown in Fig. 3 and in Ref. [42]. This rather complicated behavior of E^r should be accounted for when analyzing data in presence of RMPs, which unfortunately is often done assuming that the profile is constant along θ . In fact, E^r varies both over r and θ . The use of a helical angle to map data of E^r in a frame of reference traveling with the mode, as it is done e.g. in the stellarator or, more recently, in the RFX-mod [17, 19], could be useful for this purpose.

Our results have been obtained in the case of a static RMP: this solution is valid even in the case of slowly rotating islands, as in the case of RFX [47]. In the case of fast rotating islands (in TEXTOR, with frequency $\omega > 3$ kHz), it is necessary to account for an inductive correction for Φ , due to the term $\partial_t \alpha \vec{B}$ that adds to the expression of Eq. (5). The complete expression for this inductive correction can be found in [70], but it results in a simple Doppler shift of the potential Φ in the rotating frame of the island, which is consistent with the results by Stoschus *et al.* [15].

V. AMBIPOLAR SOLUTIONS AS A FUNCTION OF THE EDGE RADIAL ELECTRIC FIELD

As a final test, we check the ambipolarity of Φ by keeping $\tilde{\phi} = \phi$ (potential hill at the OP) and evaluating the electron and ion fluxes as a function of the potential amplitude Φ_0 , requiring $\Gamma_e = \Gamma_i$: this gives graphically the value of the ambipolar Φ_0 (or equivalently, maximum E^r). This is the algebraic way of determining the ambipolar solution, used in the stellarator community [28]. Even if the method is well-known since a long time, and its possible extension to a symmetry-breaking perturbation has already been mentioned elsewhere [27], this is the first time that the calculation has been fully carried on. To do this, we adapted ORBIT guiding center equations [41] to correctly express electron drifts. We evaluate fluxes at ψ_h , with source at $q = 4$. In Fig. 7 we plot the ion and electron fluxes as a function of Φ_0 and the maximum E^r . The two curves show two intersections $\Gamma_e = \Gamma_i$: these are known in the stellarator community as “roots”, since in the early works on the subject (such as Hastings *et al.* [28]) they actually represented the *roots* of the equations

representing the fluxes as a function of Φ' . We will maintain this terminology here, although in our case the fluxes must be evaluated numerically, similarly to the modern stellarator literature [59, 60, 61, 62]. In our simulations we find an unstable ion-root at $E^r < 0$ (~ -150 V) and a stable electron-root at $E^r > 0$ (~ 120 V), where the latter is found for a positive potential consistently with the experimental findings (see Fig. 4). This shows that two solutions are possible: one with the potential well (=maximum E^r) at the XP of the RMP (stable “electron root”, which is the solution found in experiment), and the other with the potential well at the OP (unstable, “ion root”). Here the name for the roots follows the usual meaning given in stellarators, where “electron root” means the ambipolar root for the fastest particle involved in radial transport. With the $T_e/T_i \sim 0.9$ ratio of TEXTOR, the electron root is favored, but in principle it is possible, by acting on the T_e/T_i ratio, to make the system flip to the ion root. A sensitivity scan on this point can be done with ORBIT, by varying T_e/T_i (increasing T_i), which would correspond to applying ion cyclotron resonance heating (ICRH) in an experiment. We show the D_e/D_i ratio as a function of T_e/T_i in Fig. 8, with the diffusion coefficients calculated in the OP and XP. D_e/D_i decreases by increasing T_i similarly in the OP and XP, moving from the TEXTOR experimental condition, marked as a vertical red line in the picture. In the OP the system flips to the ion root ($D_e/D_i < 1$) for $T_e/T_i \lesssim 0.5$. The opposite is seen experimentally in stellarators, where the electron root can be induced actively by electron cyclotron resonance heating (ECRH) [28]. Indeed, experimental results in the ASDEX-U and FTU tokamaks show that disruptions can be mitigated by ECRH targeted on the 2/1 island [71]. We speculate that ECRH can modify the E^r distribution in the edge, and in this way the overall magnetohydrodynamic stability at the edge: for this purpose, dedicated discharges are planned at ASDEX-U during years 2015-16, within the MST1-EUROfusion agreement [72]. In principle, the use of ECRH can be also a way of overcoming the density limit, which critically depends on the E^r pattern, at least in the RFP [48, 49]. Finally, it should be worth doing experiments of ECRH in conjunction with RMP, to assess the role of E^r on plasma stability with respect to the so-called edge localized modes [25].

VI. CONCLUSIONS

In summary, we analyzed the local radial particle transport along a helical path from the OP through the XP of an $m/n = 4/1$ remnant island, created near the edge of TEXTOR. Electron diffusion is strongly modulated (larger at the XP, lower at the OP), which requires a large electrostatic potential to ensure quasi-neutrality. We developed a 3D model for the ambipolar potential on the basis of the geometry of the remnant island: the resulting E^r shows a large positive value near the LCFS, confirming a well-known result in the RMP tokamak community. The mechanism of ambipolarity shows two possible solutions (“roots“), which suggests a way of acting on the edge E^r through additional heating.

Acknowledgments

This work has received funding from the European Union’s Horizon 2020 research and innovation programme under grant agreement number 633053 as Enabling Research Project CfP-WP14-ER-01/ENEARFX-01, and in part by Start-Up funds of the Department of Engineering Physics at the University of Wisconsin-Madison and from the U.S. Department of Energy Grants DE-AC02-09CH11466 and DE-SC00013911. One of the authors (G.S.) would like to dedicate this work to the birth of his son Marco.

-
- [1] V. P. Frolov, Phys. Rev. D **85**, 024020 (2012).
 - [2] D. L. Meier, New Astronomy Reviews **47**, 667 (2003).
 - [3] T. E. Evans, R. A. Moyer, K. H. Burrell, M. E. Fenstermacher, I. Joseph, A. W. Leonard, T. H. Osborne, G. D. Porter, M. J. Schaffer, P. B. Snyder, et al., Nature Phys. **2**, 419 (2006).
 - [4] O. Schmitz, T. E. Evans, M. E. Fenstermacher, E. A. Unterberg, M. E. Austin, B. D. Bray, N. H. Brooks, H. Frerichs, M. Groth, M. W. Jakubowski, et al., Phys. Rev. Lett. **103**, 165005 (2009).
 - [5] Y. Liang, H. R. Koslowski, P. R. Thomas, E. Nardon, B. Alper, P. Andrew, Y. Andrew, G. Arnoux, Y. Baranov, M. Bécoulet, et al., Phys. Rev. Lett. **98**, 265004 (2007).
 - [6] W. Suttrop, T. Eich, J. C. Fuchs, S. Günter, A. Janzer, A. Herrmann, A. Kallenbach, P. T. Lang, T. Lunt, M. Maraschek, et al., Phys. Rev. Lett. **106**, 225004 (2011).

- [7] J. Canik, R. Maingi, T. Evans, R. Bell, S. Gerhardt, H. Kugel, B. LeBlanc, J. Manickam, J. Menard, T. Osborne, et al., *Nuclear Fusion* **50**, 034012 (2010).
- [8] A. Kirk, I. Chapman, Y. Liu, P. Cahyna, P. Denner, G. Fishpool, C. Ham, J. Harrison, Y. Liang, E. Nardon, et al., *Nuclear Fusion* **53**, 043007 (2013).
- [9] Y. M. Jeon, J.-K. Park, S. W. Yoon, W. H. Ko, S. G. Lee, K. D. Lee, G. S. Yun, Y. U. Nam, W. C. Kim, J.-G. Kwak, et al., *Phys. Rev. Lett.* **109**, 035004 (2012).
- [10] R. Chen, G. Xu, Y. Liang, H. Wang, C. Zhou, A. Liu, L. Wang, J. Qian, K. Gan, J. Yang, et al., *Nuclear Fusion* **55**, 033012 (2015).
- [11] I. Chapman, M. Becoulet, T. Bird, J. Canik, M. Cianciosa, W. Cooper, T. Evans, N. Ferraro, C. Fuchs, M. Gryaznevich, et al., *Nuclear Fusion* **54**, 083006 (2014).
- [12] I. Chapman, D. Brunetti, P. Buratti, W. Cooper, J. Graves, J. Harrison, J. Holgate, S. Jardin, S. Sabbagh, K. Tritz, et al., *Nuclear Fusion* **54**, 083007 (2014).
- [13] S. Ortolani and D. Schnack, *Magnetohydrodynamics of Plasma Relaxation* (World Scientific, Singapore, 1993), pp. 96–103.
- [14] R. Moyer, M. Van Zeeland, D. Orlov, A. Wingen, T. Evans, N. Ferraro, J. Hanson, R. Nazikian, M. Wade, and L. Zeng, *Nuclear Fusion* **52**, 123019 (2012).
- [15] H. Stoschus, O. Schmitz, H. Frerichs, D. Reiser, M. Jakubowski, B. Unterberg, M. Lehnen, D. Reiter, U. Samm, and the TEXTOR team, *Nuclear Fusion* **52**, 083002 (2012).
- [16] P. Scarin, N. Vianello, M. Agostini, G. Spizzo, M. Spolaore, M. Zuin, S. Cappello, L. Carraro, R. Cavazzana, G. De Masi, et al., *Nuclear Fusion* **51**, 073002 (2011).
- [17] N. Vianello, G. Spizzo, M. Agostini, P. Scarin, L. Carraro, R. Cavazzana, G. De Masi, E. Martines, B. Momo, C. Rea, et al., *Nuclear Fusion* **53**, 073025 (2013).
- [18] M. Agostini, P. Scarin, G. Spizzo, N. Vianello, and L. Carraro, *Plasma Physics and Controlled Fusion* **56**, 095016 (2014).
- [19] N. Vianello, C. Rea, M. Agostini, R. Cavazzana, G. Ciaccio, G. D. Masi, E. Martines, A. Mazzi, B. Momo, G. Spizzo, et al., *Plasma Physics and Controlled Fusion* **57**, 014027 (2015).
- [20] Y. Feng, M. Kobayashi, T. Lunt, and D. Reiter, *Plasma Physics and Controlled Fusion* **53**, 024009 (2011).
- [21] K. Kamiya, K. Ida, M. Yoshinuma, C. Suzuki, Y. Suzuki, M. Yokoyama, and the LHD Experiment Group, *Nuclear Fusion* **53**, 013003 (2013).
- [22] S. Mordijck, R. Moyer, N. Ferraro, M. Wade, and T. Osborne, *Nuclear Fusion*

- [54](#), [082003](#) (2014).
- [23] P. Tamain, A. Kirk, E. Nardon, B. Dudson, B. Hnat, and the MAST team, *Plasma Physics and Controlled Fusion* [52](#), [075017](#) (2010).
- [24] P. B. Snyder, H. R. Wilson, J. R. Ferron, L. L. Lao, A. W. Leonard, T. H. Osborne, A. D. Turnbull, D. Mossessian, M. Murakami, and X. Q. Xu, *Physics of Plasmas* (1994-present) [9](#), [2037](#) (2002).
- [25] P. Lang, A. Loarte, G. Saibene, L. Baylor, M. Becoulet, M. Cavinato, S. Clement-Lorenzo, E. Daly, T. Evans, M. Fenstermacher, et al., *Nuclear Fusion* [53](#), [043004](#) (2013).
- [26] H. Renner, J. Boscary, V. Erckmann, H. Greuner, H. Grote, J. Sapper, E. Speth, F. Wesner, M. Wanner, and the W7-X Team, *Nuclear Fusion* [40](#), [1083](#) (2000).
- [27] J. Callen, *Nuclear Fusion* [51](#), [094026](#) (2011).
- [28] D. Hastings, W. Houlberg, and K. Shaing, *Nuclear Fusion* [25](#), [445](#) (1985).
- [29] O. Neubauer, G. Czymek, B. Giesen, P. W. Hüttemann, M. Sauer, W. Schalt, and J. Schruoff, *Fus. Sci. Technol.* [47](#), [76](#) (2005).
- [30] S. Abdullaev, *Magnetic Stochasticity in Magnetically Confined Fusion Plasmas* (Springer Heidelberg, 2014), vol. 78 of *Springer Series on Atomic, Optical, and Plasma Physics*.
- [31] T. Eich, D. Reiser, and K. Finken, *Nuclear Fusion* [40](#), [1757](#) (2000).
- [32] M. Lehnen, S. Abdullaev, W. Biel, M. F. M. de Bock, S. Brezinsek, C. Busch, I. Classen, K. H. Finken, M. von Hellermann, S. Jachmich, et al., *Plasma Physics and Controlled Fusion* [47](#), [B237](#) (2005).
- [33] M. Jakubowski, S. Abdullaev, K. Finken, and the TEXTOR Team, *Nuclear Fusion* [44](#), [S1](#) (2004).
- [34] M. W. Jakubowski, O. Schmitz, S. S. Abdullaev, S. Brezinsek, K. H. Finken, A. Krämer-Flecken, M. Lehnen, U. Samm, K. H. Spatschek, B. Unterberg, et al. (the TEXTOR Team), *Phys. Rev. Lett.* [96](#), [035004](#) (2006).
- [35] O. Schmitz, M. Jakubowski, H. Frerichs, D. Harting, M. Lehnen, B. Unterberg, S. Abdullaev, S. Brezinsek, I. Classen, T. Evans, et al., *Nuclear Fusion* [48](#), [024009](#) (2008).
- [36] O. Schmitz, J. Coenen, H. Frerichs, M. Kantor, M. Lehnen, B. Unterberg, S. Brezinsek, M. Clever, T. Evans, K. Finken, et al., *Journal of Nuclear Materials* [390–391](#), [330](#) (2009).
- [37] K. H. Finken, S. S. Abdullaev, M. W. Jakubowski, M. F. M. de Bock, S. Bozhenkov, C. Busch, M. von Hellermann, R. Jaspers, Y. Kikuchi, A. Krämer-Flecken, et al. (the TEXTOR team),

- Phys. Rev. Lett. **98**, 065001 (2007).
- [38] J. Coenen, O. Schmitz, B. Unterberg, M. Clever, M. Jakubowski, U. Samm, B. Schweer, H. Stoschus, M. Tokar, and the TEXTOR-Team, Nuclear Fusion **51**, 063030 (2011).
- [39] O. Schmitz, M. Kobayashi, S. Brezinsek, T. E. Evans, H. Funaba, M. Goto, K. Ida, O. Mitarai, T. Morisaki, G. Motojima, et al. (2015), submitted to Nuclear Fusion.
- [40] G. Telesca, E. Delabie, O. Schmitz, S. Brezinsek, K. Finken, M. von Hellermann, M. Jakubowski, M. Lehnen, Y. Liang, A. Pospieszczyk, et al., Journal of Nuclear Materials **390–391**, 227 (2009).
- [41] R. B. White and M. S. Chance, Physics of Fluids **27**, 2455 (1984).
- [42] G. Ciaccio, O. Schmitz, S. Abdullaev, H. Frerichs, M. Agostini, P. Scarin, G. Spizzo, N. Vianello, and R. B. White, Nuclear Fusion **54**, 064008 (2014).
- [43] T. E. Evans J. S. de Grassie, G. L. Jackson, N. Ohyabu, F. Karger, G. Haas, A. J. Wootton, K. W. Gentle, S. M. Mc Cool, W. L. Rowan, et al., in *Proc. of the 14th EPS Conference on Plasma Physics*, edited by F. Engelmann and J. L. Alvarez Rivas (European Physical Society (Petit Lancy), Madrid, Spain, 1987), vol. 11D, pp. 770–773.
- [44] S. McCool, A. Wootton, M. Kotschenreuther, A. Audemir, R. Bravenec, J. DeGrassie, T. Evans, R. Hickok, B. Richards, W. Rowan, et al., Nuclear Fusion **30**, 167 (1990).
- [45] S. Takamura, N. Ohnishi, H. Yamada, and T. Okuda, Physics of Fluids (1958-1988) **30**, 144 (1987).
- [46] K. Ida, S. Inagaki, N. Tamura, T. Morisaki, N. Ohyabu, K. Khlopenkov, S. Sudo, K. Watanabe, M. Yokoyama, T. Shimozuma, et al., Nuclear Fusion **44**, 290 (2004).
- [47] G. Spizzo, N. Vianello, R. B. White, S. S. Abdullaev, M. Agostini, R. Cavazzana, G. Ciaccio, M. E. Puiatti, P. Scarin, O. Schmitz, et al., Physics of Plasmas (1994-present) **21**, 056102 (2014).
- [48] M. Puiatti, M. Valisa, M. Agostini, F. Auriemma, F. Bonomo, L. Carraro, A. Fassina, M. Gobbin, R. Lorenzini, B. Momo, et al., Nuclear Fusion **51**, 073038 (2011).
- [49] G. Spizzo, G. Pucella, O. Tudisco, M. Zuin, M. Agostini, E. Alessi, F. Auriemma, W. Bin, P. Buratti, L. Carraro, et al., Nuclear Fusion **55**, 043007 (2015).
- [50] K. C. Shaing, Physics of Plasmas (1994-present) **9**, 3470 (2002).
- [51] K. Shaing, C. Hegna, J. Callen, and W. Houlberg, Nuclear Fusion **43**, 258 (2003).
- [52] A. H. Boozer, Physics of Fluids **24**, 1999 (1981).

- [53] R. B. White, G. Spizzo, and M. Gobbin, *Plasma Physics and Controlled Fusion* **55**, 115002 (2013).
- [54] G. Ciaccio, M. Veranda, D. Bonfiglio, S. Cappello, G. Spizzo, L. Chacon, and R. B. White, *Physics of Plasmas* **20**, 062505 (pages 12) (2013).
- [55] M. Kobayashi, Y. Feng, F. Sardei, D. Reiter, K. Finken, and D. Reiser, *Nuclear Fusion* **44**, S64 (2004).
- [56] G. Spizzo, R. B. White, and S. Cappello, *Physics of Plasmas* **14**, 102310 (pages 8) (2007).
- [57] R. B. White, *The theory of toroidally confined plasmas* (Imperial College Press, London, 2014), p. 46, 3rd ed.
- [58] G. Spizzo, R. B. White, S. Cappello, and L. Marrelli, *Plasma Physics and Controlled Fusion* **51**, 124026 (2009).
- [59] S. Satake, Y. Idomura, H. Sugama, and T.-H. Watanabe, *Computer Physics Communications* **181**, 1069 (2010).
- [60] S. Matsuoka, S. Satake, M. Yokoyama, A. Wakasa, and S. Murakami, *Physics of Plasmas* **18**, 032511 (pages 11) (2011).
- [61] J. M. García-Regaña, R. Kleiber, C. D. Beidler, Y. Turkin, H. Maaßberg, and P. Helander, *Plasma Physics and Controlled Fusion* **55**, 074008 (2013).
- [62] J. Lore, W. Guttenfelder, A. Briesemeister, D. T. Anderson, F. S. B. Anderson, C. B. Deng, K. M. Likin, D. A. Spong, J. N. Talmadge, and K. Zhai, *Physics of Plasmas* (1994-present) **17**, 056101 (2010).
- [63] Y. Xu, M. V. Schoor, R. Weynants, S. Jachmich, M. Vergote, M. Jakubowski, P. Beyer, M. Mitri, B. Schweer, D. Reiser, et al., *Nuclear Fusion* **47**, 1696 (2007).
- [64] W. R. Hess, C. DeMichelis, M. Mattioli, F. Clairet, M. Druetta, A. Grosman, R. Guirlet, T. Hutter, J. Lasalle, and P. Monier-Garbet, *Plasma Physics and Controlled Fusion* **37**, 951 (1995).
- [65] V. Rozhansky, E. Kaveeva, P. Molchanov, I. Veselova, S. Voskoboynikov, D. Coster, A. Kirk, S. Lisgo, and E. Nardon, *Nuclear Fusion* **50**, 034005 (2010).
- [66] Y. Xu, R. R. Weynants, S. Jachmich, M. Van Schoor, M. Vergote, P. Peleman, M. W. Jakubowski, M. Mitri, D. Reiser, B. Unterberg, et al. (the TEXTOR team), *Phys. Rev. Lett.* **97**, 165003 (2006).
- [67] E. Kaveeva and V. Rozhansky, *Technical Physics Letters* **30**, 538 (2004).

- [68] G. D. Conway, S. Fietz, H. W. Müller, T. Lunt, P. Simon, W. Suttrop, M. Maraschek, T. Hapfel, and E. Viezzer, *Plasma Physics and Controlled Fusion* **57**, 014035 (2015).
- [69] K. Ida, N. Ohya, T. Morisaki, Y. Nagayama, S. Inagaki, K. Itoh, Y. Liang, K. Narihara, A. Y. Kostrioukov, B. J. Peterson, et al. (LHD Experimental Group), *Phys. Rev. Lett.* **88**, 015002 (2001).
- [70] R. B. White, *The theory of toroidally confined plasmas* (Imperial College Press, London, 2014), p. 227, 3rd ed.
- [71] B. Esposito, G. Granucci, P. Smeulders, S. Nowak, J. R. Martín-Solís, and L. Gabellieri (FTU and ECRH teams), *Phys. Rev. Lett.* **100**, 045006 (2008).
- [72] M. Maraschek, B. Esposito, and G. Granucci, *Disruption control in high β_n and high density scenarios with ECCD/ECRH*, AUG proposal 15-1.3-3, URL http://users.euro-fusion.org/iterphysicswiki/index.php/WPMST1_2015.Proposals.

Figure Captions

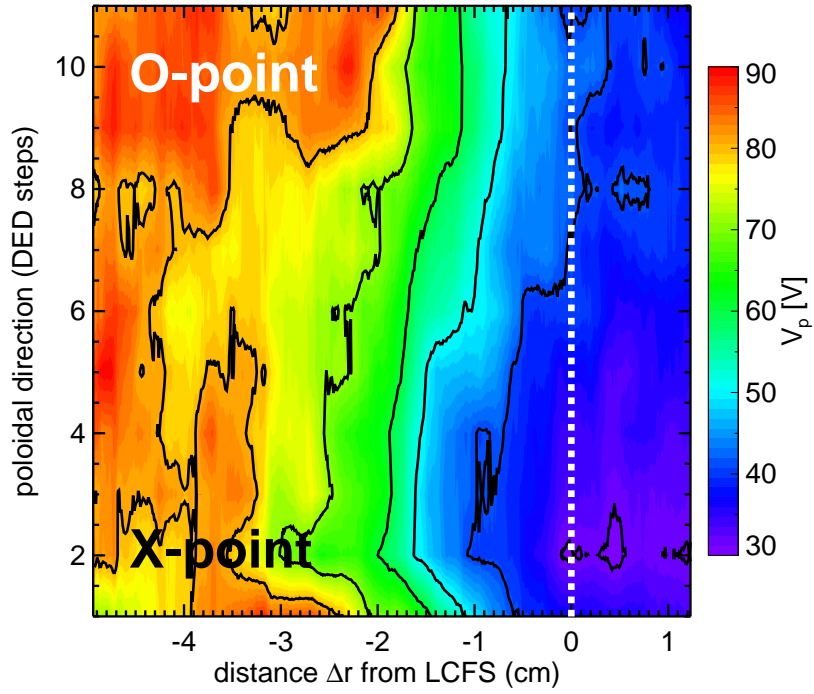


FIG. 1: Contour map of the plasma potential, measured with a sweeping probe in TEXTOR edge. On x-axis, the radial distance from the LCFS (in cm), on the y-axis the poloidal direction, measured as "steps" in the DED phase of the 4/1 island. The approximate positions of the island O- and X-points are labeled on the contour map.

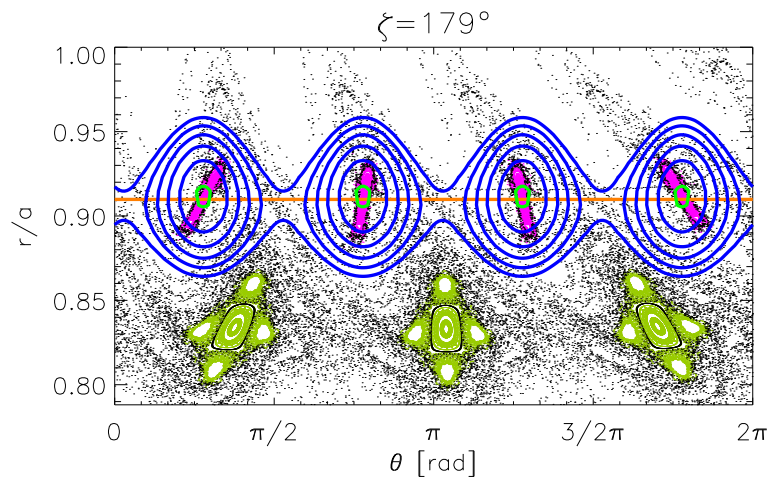


FIG. 2: Poincaré plot of the vacuum magnetic field lines, superimposed to the helical 4/1 flux surfaces, $\psi_h^{(4,1)}$ (blue curves). The x-axis is the poloidal angle while the y-axis is the normalized radius.

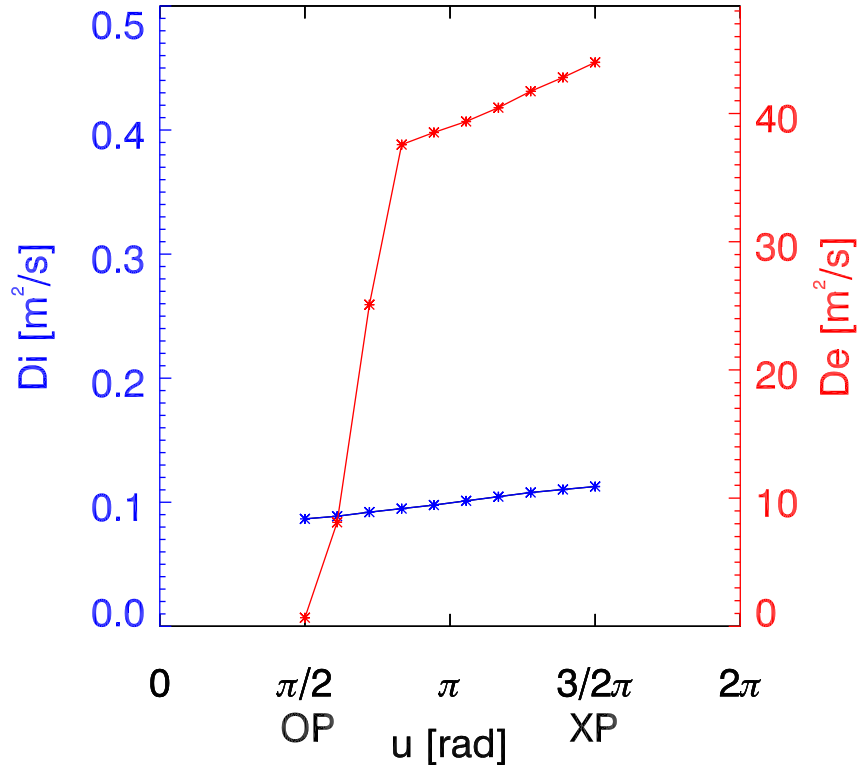


FIG. 3: D_i and D_e values along the helical flux in between the OP and XP at $3\pi/2$. On the x-axis the helical angle $u = m\theta - n\zeta + \phi$.

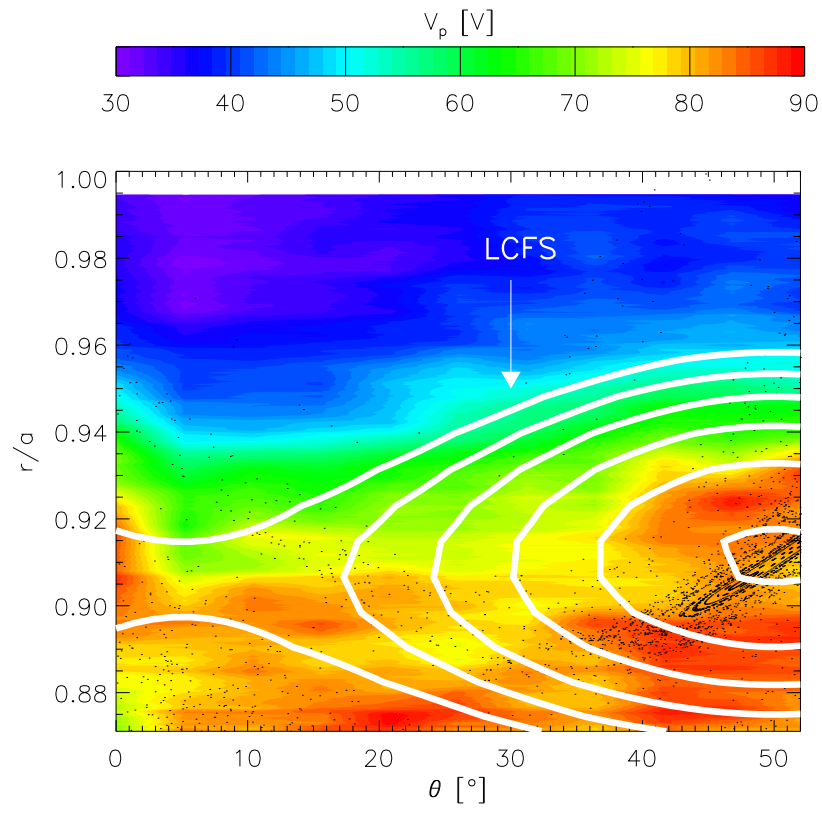


FIG. 4: Map of the measured plasma potential V_p remapped onto the flux surfaces of the 4/1 island, on the θ, r plane. The helical flux surfaces $\psi_h^{(4,1)}$ (white contours) and the magnetic field Poincaré plot (points) are overplotted.

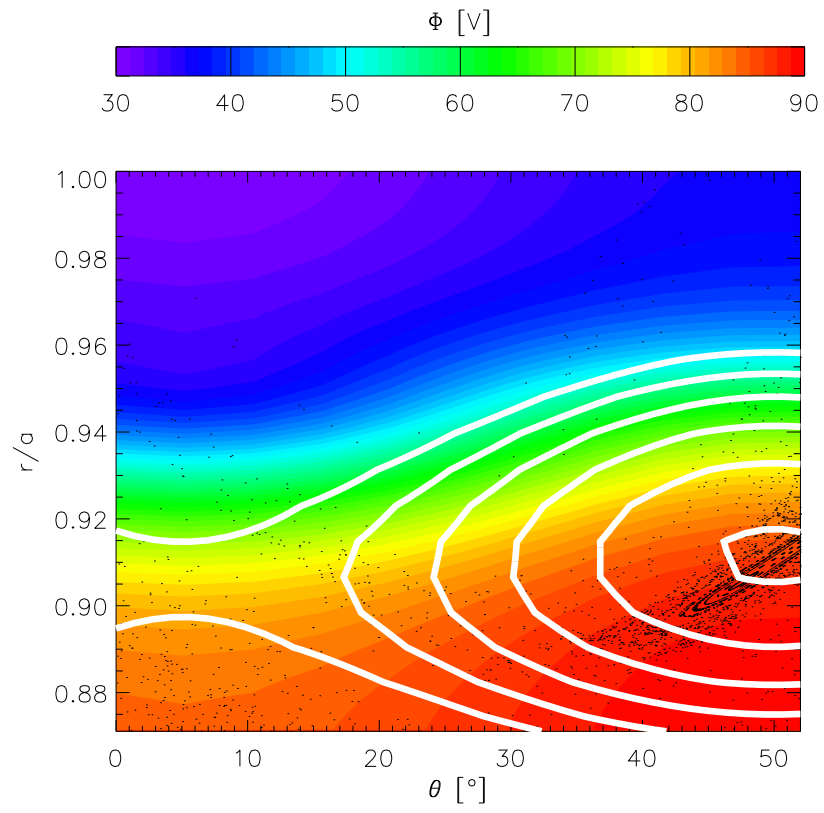


FIG. 5: Map of the modeled potential, Φ , in the (θ, r) plane.

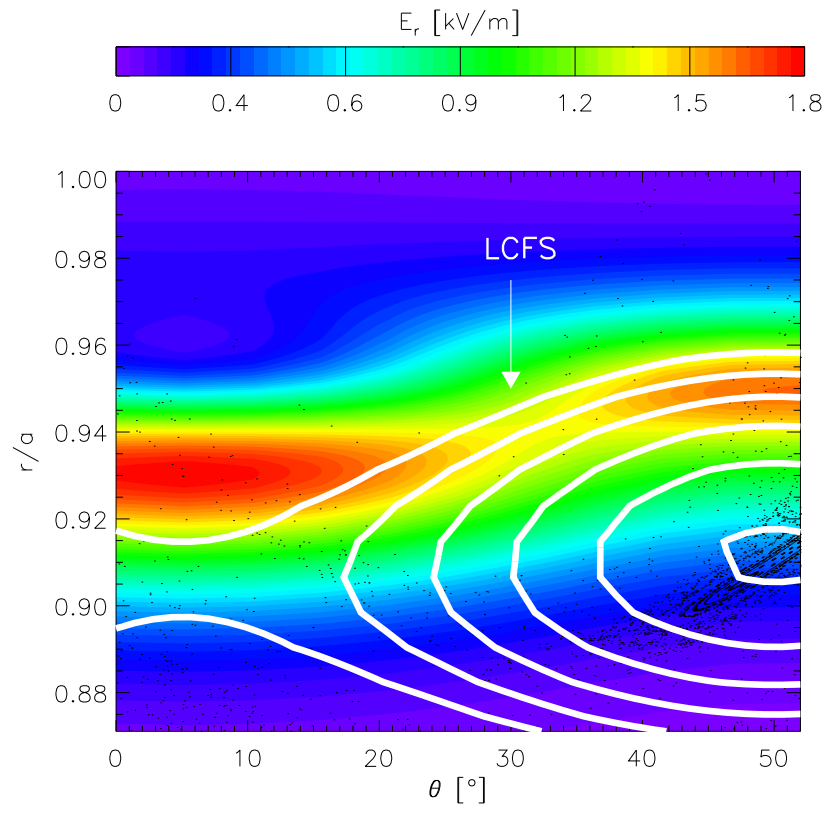


FIG. 6: Map of the modeled E_r in the (θ, r) plane.

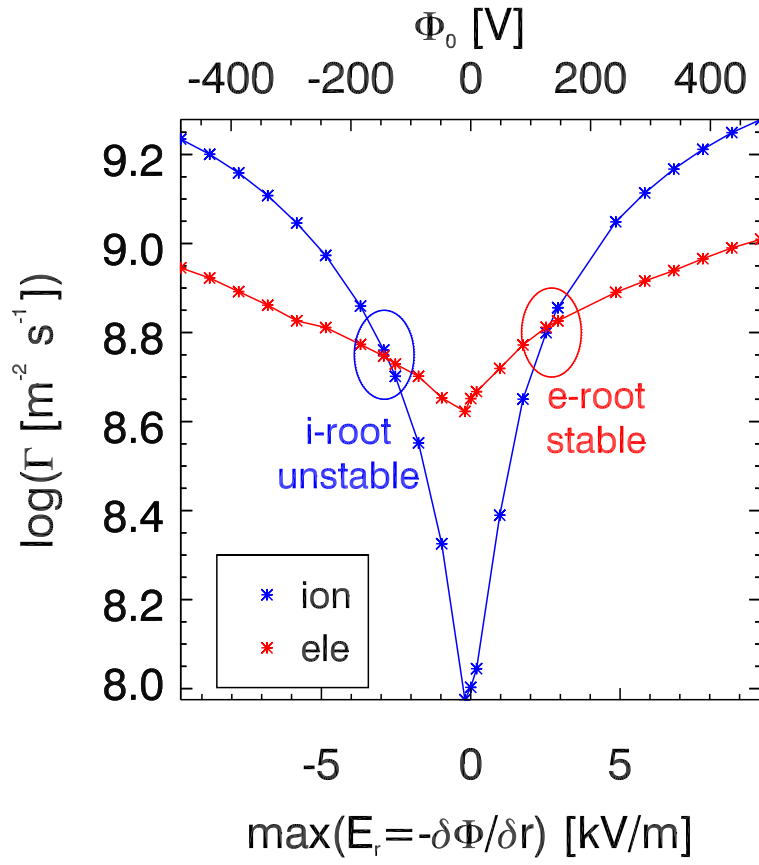


FIG. 7: Ion (blue) and electron (red) fluxes as a function of Φ_0 and the maximum E^r .

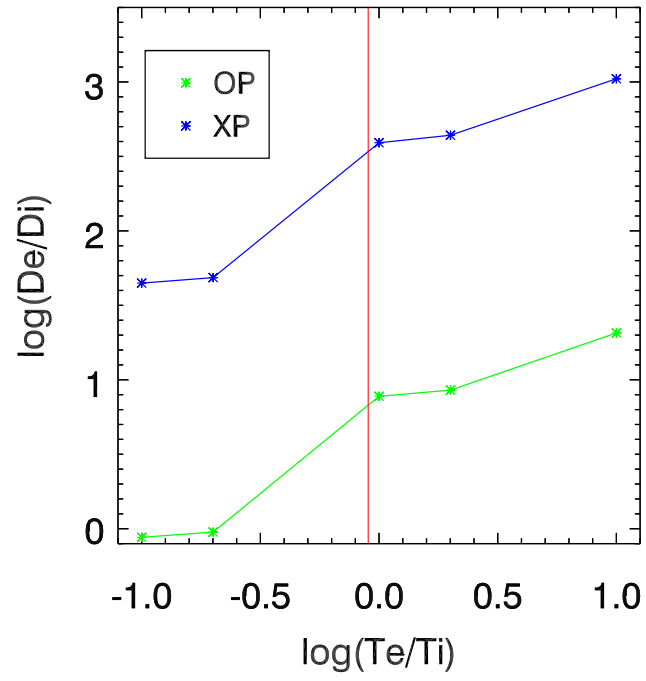


FIG. 8: D_e/D_i as a function of T_e/T_i calculated in the OP and XP.